Angiogenesis (2026) 29:15
https://doi.org/10.1007/s10456-025-10027-3

ORIGINAL PAPER

Endothelial USP8 is essential for angiogenesis

Alba Pau-Navalón[1,2] · Tamara González-Costa[1,2] · María Lancho Lavilla[1] · Andrés A. Urrutia[3] · José Luis de la Pompa[1,2] · Henar Cuervo[4] · Joaquim Grego-Bessa[1,2,5,6]

Received: 9 April 2025 / Accepted: 9 December 2025

Abstract

Angiogenesis, the formation of new blood vessels from existing ones, is crucial for both development and disease. Its dysregulation is associated with diseases such as cancer, obesity, and blindness. Vascular endothelial growth factor A (VEGFA) signaling through VEGF receptor 2 (VEGFR2) is the central regulator of angiogenesis. Consequently, there is significant interest in identifying modulators of this pathway to develop targeted therapeutic interventions. Ubiquitination tags proteins for degradation, whereas deubiquitinases counteract this process by removing the attached ubiquitin molecules. Previous studies have shown that the deubiquitinase Ubiquitin-Specific Protease 8 (USP8) regulates VEGFR2 trafficking and activation in vitro, suggesting that USP8 may regulate endothelial cell function. To examine the role of endothelial USP8 in angiogenesis in vivo, we used conditional mouse genetics to delete Usp8 in endothelial cells at different stages: during embryonic development, after birth, and in adulthood. Loss of endothelial *Usp8* during embryogenesis resulted in impaired intersomitic vessel angiogenesis and lethality by E10.5. Early postnatal deletion caused severe defects in retinal angiogenesis and abnormal brain vasculature, while adult deletion had no overt vascular effects. Impaired angiogenesis in endothelial *Usp8* deficient mice was associated with decreased endothelial cell-cycle activation and increased vessel diameter in capillaries and veins. Mechanistically, we found that loss of endothelial *Usp8* led to VEGFR2 accumulation in early endosome aggregates and reduced phospho-ERK signaling. Our findings identify endothelial USP8 as a key regulator of angiogenesis across developmental and postnatal contexts, while dispensable for endothelial homeostasis in adulthood, highlighting its potential as a therapeutic target for anti-angiogenic interventions.

Keywords VEGFR2 · Deubiquitinases · Vessel formation · Angiogenesis · USP8

✉ José Luis de la Pompa
jlpompa@cnic.es

✉ Henar Cuervo
hcuervo@cnic.es

✉ Joaquim Grego-Bessa
jgrego@carrerasresearch.org

[1] Intercellular Signalling in Cardiovascular Development and Disease Laboratory CNIC, Centro Nacional de Investigaciones Cardiovasculares Carlos III (F.P.S), Madrid, Spain

[2] CIBER de Enfermedades Cardiovasculares (CIBERCV), Madrid, Spain

[3] Research Unit, Research Institute Princesa (IIS IP), Hospital of Santa Cristina, Universidad Autónoma de Madrid, 28009 Madrid, Spain

[4] Molecular Genetics of Angiogenesis Laboratory CNIC, Centro Nacional de Investigaciones Cardiovasculares Carlos III (F.P.S), Madrid, Spain

[5] Endothelial Pathobiology and Microenvironment, Josep Carreras Leukaemia Research Institute, Badalona, Spain

[6] Advanced Microscopy Unit, Institut de Recerca Contra la Leucèmia Josep Carreras (IJC), ICO-Hospital Germans Trias i Pujol, Universitat Autònoma de Barcelona, Barcelona, Spain

Published online: 28 January 2026

Introduction

Angiogenesis is the process of forming new blood vessels from preexisting ones. This essential step in development is finely regulated to establish a hierarchical vascular network that supplies tissues with oxygen and nutrients [1]. In various pathological conditions—such as cancer, stroke, diabetic retinopathy, and age-related macular degeneration—this regulation is disrupted, leading to either excessive or insufficient blood vessel formation [2].

During angiogenesis, endothelial cells detach from their parent vessel and migrate to hypoxic sites. Tip cells lead the way, followed by stalk endothelial cells that proliferate to expand the vascular plexus. Once an immature plexus forms, vessel remodeling, endothelial stabilization, and arteriovenous differentiation occur, ultimately creating a functional, mature vascular network [1]. Hypoxia-driven vascular endothelial growth factor A (VEGF) is a major regulator of all these steps and it exerts most of its functions through interaction with the VEGF receptor 2 (VEGFR2) [3].

VEGF-VEGFR2 signaling is tightly regulated at multiple levels, including transcriptional regulation, protein processing, ligand interaction, endocytosis, and trafficking [4]. Upon ligand binding, VEGFR2 dimerizes, leading to the phosphorylation of intracellular tyrosine residues, which initiate various signaling cascades essential for endothelial function [5]. VEGFR2-ligand interaction also triggers receptor endocytosis into early endosomes (EEs) [6]. This internalization and intracellular trafficking are critical for regulating signaling output [7]. Consequently, ERK1/2 activation, which is essential for VEGFR2 signaling and endothelial biology, is reduced when receptor trafficking is impaired [8].

Ubiquitination is a reversible and dynamic posttranslational modification that regulates multiple cellular processes. Deubiquitinases (DUBs) are proteases that remove ubiquitin residues from ubiquitinated proteins. Together, ubiquitination and deubiquitination form a complex ubiquitin code that, not only targets proteins for proteasomal degradation, but also plays non-degradative roles in cellular signaling and intracellular trafficking [9]. In membrane receptors, the removal of ubiquitin residues can influence their degradation, signaling and recycling [10]. For VEGFR2, once internalized, ubiquitination regulates its endosomal sorting determining whether its recycled back to the plasma membrane or degraded via the lysosomal-proteasome system [11]. DUBs reverse ubiquitin signals with equally high sophistication.

Ubiquitin-Specific Protease 8 (USP8) is a DUB known to regulate VEGFR2 trafficking. Deficiency of USP8 in endothelial cells in vitro results in a defective degradation and receptor trafficking affecting VEGF induced ERK activation [12]. Despite the critical role of USP8 in regulating VEGFR2 functions, it remains unclear to what extent this regulation impacts endothelial cell functions during angiogenesis and how the cellular and biochemical environment of an organism influences its biological significance. Here, we demonstrate that endothelial USP8 is essential for normal angiogenesis, exerting organ-specific effects. *Usp8* inactivation in endothelial cells disrupts angiogenesis and leads to abnormal vascular network formation. *Usp8*-deficient endothelial cells exhibit reduced numbers, impaired VEGFR2 trafficking, and diminished ERK activation. Together, our findings reveal that USP8 plays a crucial role in endothelial cell function, ensuring proper angiogenic processes.

Materials and methods

Mouse lines

Animal studies were approved by the CNIC Animal Experimentation Ethics Committee and by the Community of Madrid (Ref. 10/249364.9/25). All animal procedures conformed to EU Directive 2010/63EU and Recommendation 2007/526/EC regarding the protection of animals used for experimental and other scientific purposes, enacted in Spanish law under Real Decreto 118/2021 (modification on Real Decreto 53/2013) and Ley 32/2007. To study the role of USP8 in vascular development, we used mice with a conditional $Usp8^{flox}$ allele [13] containing two *loxP* sites flanking the exons 3 and 4 of the *Usp8* gene. $Usp8^{flox}$ mice were combined with the *Tie2Cre* mouse line [14], which expresses Cre recombinase driven by the *Tie2* promoter, and with *Cdh5-CreER*^{T2} mice [15], which expresses tamoxifen-inducible Cre-Recombinase in the vascular endothelium. The reporter mouse line *mTmG* ($R26^{mT/mG}$) [16] was used to assess Cre-mediated recombination. All mice were maintained in a C57BL/6 inbred background. Primer sequences for genotyping can be found in Supplementary Table 1.

To constitutively delete *Usp8* in endothelial cells, we crossed $Usp8^{flox/flox}$ or $Usp8^{flox/flox}$;$R26^{mTmG}$ females with $Usp8^{flox/wt}$;*Tie2-Cre* males. To analyze postnatal and adult vasculature we crossed $Usp8^{flox/flox}$;$R26^{mT/mG}$ females with $Usp8^{flox/flox}$;*Cdh5-CreER*^{T2};$R26^{mTmG}$ *or* $Usp8^{flox/flox}$;*Cdh5-CreER*^{T2} males. For postnatal studies, 20 µl of a 5 mg/mL solution of 4-Hydroxytamoxifen (4-OHT; Sigma-Aldrich H6278) was administered intraperitoneally (i.p.) at postnatal day (P)1 and P2. For adult induction studies, 100 µl of 5 mg/mL solution of Tamoxifen (Sigma-Aldrich T5648) was administered i.p. at 6 weeks, during 4 consecutive days.

Whole embryo analysis

Embryos were dissected at embryonic day (E)9.5 and were sorted according to somite number to ensure comparable developmental stages in all experiments with control and mutant embryos. E9.5 embryos expressing eGFP derived from the *mTmG* allele were fixed in 4% formaldehyde in phosphate buffer solution (PBS) for 2 h at 4 °C. After several washes in PBS, whole embryos were stained with anti-GFP (Aves Labs GFP-1010) and mounted on BRAND cavity slides (Merck BR475505) using Vectashield mounting media (Vector H-1000).

Histology and immunostainings

Embryos were fixed 5 h. in 4% formaldehyde in PBS at 4 °C. Organs from postnatal or adult mice were fixed for 24–48 h., respectively, in 4% formaldehyde in PBS at 4 °C. For cryosections, samples were soaked in 30% sucrose, embedded in optimal cutting temperature (OCT) compound and stored at −80 °C. For paraffin sections, samples were dehydrated through a graded ethanol series followed by xylene washes and embedded in paraffin at 65 °C. 10 µm OCT or 7 µm paraffin sections were processed for immunostaining. For phospho(p)ERK, ERG, N1ICD, and VEGFR2 staining, sections were boiled in 0.01 M Sodium Citrate solution pH = 6 for antigen retrieval. All Sections were blocked for 30 min with 0.5% Triton X-100 in PBS (0.5% PBS-TX), 5% Fetal Bovine Serum (FBS) and incubated overnight at 4 °C with primary antibodies (details in Supplementary Table 1). Sections were then washed several times in 0.3% Triton X-100, and incubated for 1 h with the appropriate fluorescent-dye-conjugated secondary antibodies (see Supplementary Table 1) diluted in the same solution. For N1ICD signal amplification, we used ImmPRESS HRP horse anti-rabbit polymer (Vector Labs, MP-7401-15). For counterstaining we used IsolectinB4 (endothelium) and DAPI (nuclei). For proliferation analysis of embryos, pregnant dams received an i.p. injection of 200 µl of 5-ethynyl-2'-deoxyuridine (EdU) (5 mg/ml). After 2 h, embryos were collected in PBS and processed for EdU immunodetection according to the manufacturer protocols. In the case of N1ICD and pERK, signal was amplified with TSA Fluorescence System tyramide kit (ApexBio, K1050). DAB staining was developed with DAB Peroxidase (HRP) Substrate Kit (Vector, SK-4100). Hematoxylin and Eosin staining was performed in 5 µm thick paraffin sections using standard protocols on the CNIC Histology Core. Sections were mounted with Fluoromount-G (Southern Biotech, 0100-01) or DPX (Sigma-Aldrich 06522).

Whole-mount Immunofluorescence

In the case of retinas, eyes were collected at postnatal day (P) 6, 12 or 14 weeks after birth and fixed in 4% formaldehyde in PBS for 30 min at room temperature. After PBS washes, retinas were micro-dissected and fixed again for 45 min in 4% formaldehyde in PBS. After washing in PBS and blocking with 0.3% PBS-TX, 5% FBS for 2 h, samples were incubated with primary antibodies overnight at 4 °C (Supplementary Table 1). After several washes in PBS, retinas were incubated for 2 h at room temperature with species-specific Alexa Fluor-coupled secondary antibodies (details in Supplementary Table 1) and counterstained using IsolectinB4. Retinas were mounted with Fluoromount-G (Southern Biotech, 0100-01). For VEGR2 staining with no permeabilization, we removed Triton X-100 from the solutions and followed described incubation times and antibody concentration.

Brains were dissected and fixed for 24 h in 4% formaldehyde in PBS at 4 °C. 150–200 µm slices from the cortex were obtained using a scalpel, washed in PBS and subsequently blocked in 0.3% PBS-TX, 5% donkey serum overnight at 4 °C. Sections were then incubated with primary antibodies (details in Supplementary Table 1) during 24 h at 4 °C in the same solution. After extensive washes in PBS, samples were incubated overnight with species-specific Alexa Flour-coupled secondary antibodies (details in Supplementary Table 1) and mounted on BRAND cavity slides (Merck BR475505) using Vectashield mounting medium (Vector H-1000).

Image acquisition and quantification

Whole brain bright field images were obtained using a Leica MZFLIII stereoscope coupled to a Nikon DP71 camera and analyzed with CellSens software. Brains exhibiting hemorrhages were categorized as positive, while those lacking hemorrhages were classified as negative.

Brightfield images from histological sections were taken in an Olympus BX51 microscope coupled to a Nikon DP71 camera and CellSens software. Fluorescence images were taken using a Leica SP8 or Leica Stellaris 8 confocal microscope and LASX software. Images were processed and analyzed with Qupath v0.6.0 or ImageJ Fiji software.

For the analysis of the E9.5 embryonic vasculature, the number of connecting vessels of intersomitic vessels was counted in 3 somites of the rostral or caudal area, and the perimeter of the cardinal vein and dorsal aorta was measured with the 'freehand selections' tool from Fiji software from embryonic sections.

Vascular density was calculated measuring the IsolectinB4 or Endomucin area with the 'create threshold' tool followed

by "Measurement" of the area. The result was normalized to the total area of the tissue. Branching points were manually counted and correlated to the vascular area. Tip cells were manually counted and correlated to the vascular front area. To assess the diameter of the vessels, the 'straight line' tool from Fiji was manually employed on auto-scaled images. The radial growth was calculated relating the progression of the vessels to the length of the retina. Endothelial cell surface area was manually measured by tracing the cell perimeter using the "Freehand Tool" in QuPath.

To determine the recombination levels, endogenous mGFP signal was quantified using the 'create threshold' tool from Fiji software, and the result was correlated to the vascular area. Similarly, smooth muscle actin (SMA) and DESMIN signal was quantified with the 'create threshold' tool and correlated to the vascular area.

For Ki67, Cleaved Caspase 3 and EdU positive nuclei detection, we used the 'cell detection' tool from Qupath software, and the identified positive cells were normalized to the total number of ERG^+ endothelial nuclei.

pERK positive cells in E9.5 embryos were manually counted in the dorsal aorta, cardinal vein and meningeal vessels and related to the total number of endothelial cells constituting the vessels. pERK signal in the retinal vasculature was quantified with the 'create threshold' tool from Fiji software and correlated to the vascular area.

VEGFR2 and Isolectin B4 signal intensity in 8-bit pictures was determined using Fiji's "RGB profile" tool, along a 10-pixel-wide line across the vessel.

Evans blue

A 2% Evans Blue stock solution was prepared in sterile normal saline (0.9% NaCl). The dye was administered intraperitoneally at a dose of 5 µL per gram of body weight to postnatal day 5 (P5) mice, and brains were harvested at postnatal day 6 (P6).

RNAscope

Commercially available RNAscope probes for *Acta2* (Catalog # 319531-C2), *USP8* (Catalog # 1305711-C1) and *Pecam* (Catalog # 316721-C3) were acquired from Biotechne. RNAscope was performed according to manufacturer instructions. For fluorescence visualization RNAscope multiplex TSA Buffer (Catalog # 322809) was used together with TSA Vivid™ Fluorophore Kit 520 (323271), TSA Vivid™ Fluorophore Kit 570 (323272), and TSA Vivid™ Fluorophore Kit 650 (323273) from Tocris.

Statistical analysis

Data were analyzed using GraphPad Prism software. We analyzed at least 3 specimens per experimental group for all experiments. Statistical analyses were performed using unpaired two-tailed Student´s T-test with Welch's correction unless otherwise specified. For hemorrhagic whole-mount brains quantification and embryonic survival, statistical significance was assessed using Fisher's exact test. Differences were considered statistically significant at $P<0.05$. Unless otherwise stated, data are presented as mean ± SD (error bars).

Results

Loss of endothelial USP8 results in abnormal vessel formation and embryonic lethality

To evaluate whether USP8 regulates endothelial cell functions in vivo we started by looking into the role of endothelial USP8 during early vascular development in mammals. For this purpose, we crossed $Usp8^{flox}$ mice [13] with the $Tie2^{Cre}$ mouse line [14], which allows to delete *Usp8* in endothelial cells. $Usp8^{flox/flox};Tie2^{Cre}$ mice exhibited expected mendelian ratios at E9.5, however, they did not survive beyond E10.5 (Fig. 1a). We focused our study of the vasculature of these mice at E9.5 when most mutant embryos appeared healthy (75%). To easily visualize the endothelium of $Usp8^{flox/flox};Tie2^{Cre}$ mice, we crossed them with mice carrying the $R26^{mT/mG}$ allele, which allows for mGFP expression under the control of Cre recombinase resulting in membrane eGFP expressing endothelial cells and therefore highlighting the vasculature. Analysis of $Usp8^{flox/flox};Tie2^{Cre};R26^{mT/mG}$ (referred to as $Usp8^{\Delta EC}$ in Fig. 1) E9.5 whole-mount embryos (stage-matched at 22–23 somites) revealed defective formation of intersomitic vessels in mutants compared to controls (Fig. 1b, c). These defects were observed in both the rostral and caudal regions (Fig. 1b', b'', c', c'', d, e) suggesting that the anomalies represent a specific impairment of angiogenesis in mutants, rather than being a consequence of delayed embryonic development. To further explore how loss of endothelial *Usp8* was affecting the vasculature, we evaluated E9.5 embryo cross-sections immunostained with anti-CD31. This analysis of the vasculature revealed a significantly increased perimeter of the cardinal vein (CV) and meningeal vessels (MV) in mutant mice compared to controls. Interestingly, no differences were observed in the perimeter of the dorsal aorta (DA) (Fig. 1f–j).

The presence of differential responses to loss of *Usp8* among vascular segments led us to investigate whether basal *Usp8* expression varies between arteries, veins, and

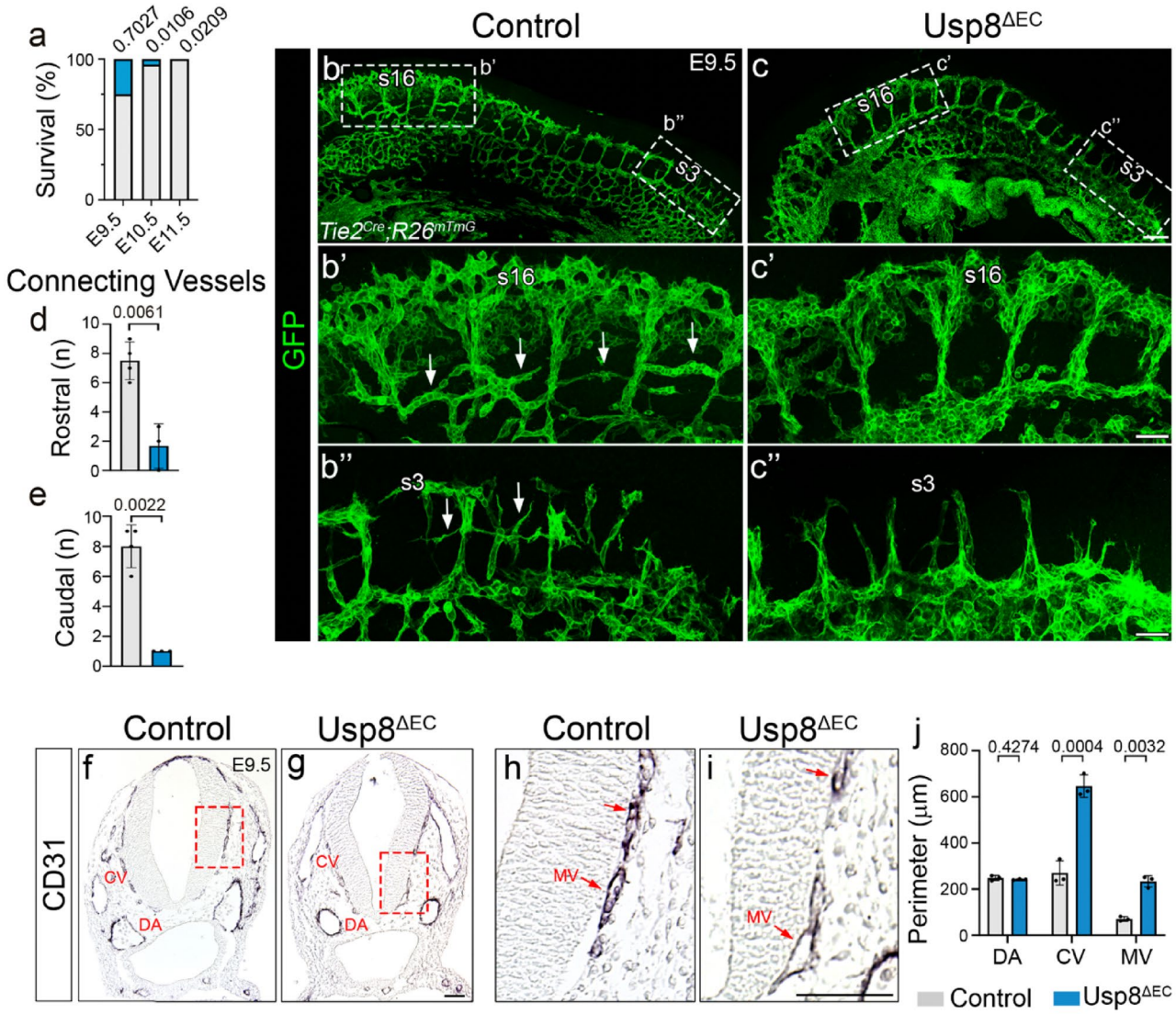

Fig. 1 Endothelial USP8 is required for embryonic angiogenesis. **a** Survival rate of Usp8$^{\Delta EC}$ (blue) and control (gray) embryos at different stages. **b**, **c** Whole-mount immunofluorescence images of mGFP expression in the trunk of control and Usp$^{\Delta EC}$ E9.5 embryos. Boxed regions show magnifications of somites (s) from control and mutant embryos: s14-s18 (**b**', **c**'), and s1–s5 (**b**" and **c**"). Arrows point to intersomitic connecting vessels. **d**, **e** Quantification of the rostral (s7–s11) and caudal (s1–s5) intersomitic connecting vessels ($n=3$ embryos per genotype). **f**, **g** CD31 immunohistochemistry on transversal sections at thoracic level of control and Usp$^{\Delta EC}$ E9.5 embryos. CV: cardinal vein, DA: dorsal aorta. **h**, **i** Magnification of boxed region in f-g; red arrows indicate meningeal vessels (MV). **j** Quantification of the perimeter of the CV, DA and MV ($n=3$ embryos per genotype; ≥ 3 sections per embryo). Bars represent mean ± S.D except for (**c**). Data were analyzed using unpaired T-test with Welch's correction. Scale bars indicate 250 µm in b–c, 100 µm in b'–c", and 50 µm in f–i

capillaries. To assess *Usp8* expression in the embryonic vasculature, we performed fluorescent in situ hybridization (FISH) using the RNAscope technology. We found that *Usp8* was ubiquitously expressed throughout the embryo, including within the vasculature. No overt differences were observed in *Usp8* signal intensity among DA, CV, or MV (Supplementary Fig. 1), suggesting that the different response to changes in perimeter among the vascular segments are not due to a differential expression of *Usp8*.

Overall, our data shows that loss of endothelial *Usp8* results in lethality after E10.5. Analysis of the vasculature during early developmental stages reveals impaired angiogenesis and dilation of the cardinal vein and meningeal vessels in mutant mice, underscoring the essential role of endothelial USP8 in embryonic vascular formation.

Endothelial USP8 regulates endothelial cell functions during retinal angiogenesis

To shed further light into the role of endothelial USP8 in angiogenesis we turned to the mouse retina. The mouse retinal vasculature develops after birth, allowing for the study of vascular angiogenesis without the lethality or potential developmental confounding effects associated with embryonic studies. For these studies, we crossed *Usp8*^{flox} mice with *Cdh5*^{CreERT2} mice, enabling tamoxifen-inducible Cre recombinase expression in endothelial cells [15]. Mutant *Usp8*$^{flox/flox}$;*Cdh5*^{CreERT2} (referred to as Usp8$^{i\Delta EC}$) and control mice were also carrying the *R26*$^{mT/mG}$ allele. Recombination of *Usp8* and the *mT/mG* cassette was induced by injection of 4OH-Tamoxifen to the pups at postnatal (P) day 1 and 2 (Fig. 2a). At P6, when retinal vessels are undergoing angiogenesis, retinas were isolated and whole-mount immunostained with IsolectinB4 to visualize endothelial cells.

Our analysis of IsolectinB4 (labels all endothelial cells) and GFP-expressing endothelial cells (Cre-expressing cells) revealed a close to 100% recombination efficiency in the case of control mice, however we observed a high variability in the levels of Cre-induced mGFP-expressing cells in Usp8$^{i\Delta EC}$ mice (Fig. 2b–e). These differences in the mGFP expressing endothelial cells were associated with differences in the severity of the vascular phenotypes observed. Therefore, for our analyses, we decided to divide the mutant mice into two groups according to their level of recombination: lower recombination (Fig. 2d–50% of the endothelium expresses mGFP), and higher recombination (Fig. 2e and 51–100% of the endothelium cells expresses mGFP).

To establish a role for endothelial USP8 in the retinal angiogenic response we evaluated the radial growth of the vascular plexus, the vascular density, the vascular branching points, and the tip cells in Usp8$^{i\Delta EC}$ compared to control mice (Fig. 2).

Our analysis revealed a reduction in all these parameters in mutant mice with low recombination, which was even more pronounced in the group of mutant mice with a higher recombination percentage (Fig. 2c–i). We also evaluated vessel diameter in the different vascular segments: arteries, capillaries and veins. This severely abnormal vascular plexus did not allow for the morphological distinction of arteries and veins, which were only measured in low recombination mutants and control mice. We observed an increased diameter in the case of the veins and the capillary segments, but no changes were detected in the arterial compartment (Fig. 2j).

Mural cells (vascular smooth muscle cells and pericytes) are perivascular cells that interact with the endothelium and stabilize the vasculature during the angiogenic process [3]. To determine whether mural cells were altered following endothelial deletion of *Usp8*, we immunostained the retinas of control and mutant mice with anti-smooth muscle actin (SMA) to visualize vascular smooth muscle cells (vSMCs), and with anti-desmin to visualize pericytes and vSMCs. Our analysis did not reveal any differences in the vascular coverage of vSMCs (Supplementary Fig. 2a–c) or pericytes (Supplementary Fig. 2d–g). Overall, our findings show that loss of endothelial *Usp8* postnatally leads to an impaired angiogenesis of the retinal vasculature characterized by reduced vascular density and growth together with an increase in diameter of the capillaries and venous vascular segments.

Fig. 2 Endothelial USP8 is required for retinal angiogenesis. **a** Experimental design. **b** Percentage of vessel area expressing mGFP in whole-mount retinas, grouped by control, low and high recombination (n ≥ 8 retinas per genotype). **c–e** Whole-mount immunofluorescence staining with IsolectinB4 (IB4, gray) and **c'–e'** mGFP expression (green) of P6 retinas from control (gray box) and Usp$^{i\Delta EC}$ mice with low (light blue box) and high (dark blue box) levels of mGFP recombination. Quantification of **f** vascular density, **g** branching points, **h** radial growth **i** tip cells, and **j** diameter of arteries, veins and capillaries of P6 control and Usp$^{i\Delta EC}$ retinas ($n \geq 5$ retinas per genotype). Bars represent mean ± S.D. Data were analyzed using unpaired T-test with Welch's correction. Scale bar indicates 500 µm

Postnatal loss of endothelial Usp8 differentially affects the vasculature of several organs

In addition to the postnatal retinal vasculature, we also evaluated brain, lungs, heart and liver from control and mutant mice to study the potential role of endothelial *Usp8* in other vascular beds (Fig. 3a and Supplementary Fig. 3). Upon dissection we did not observe any overt differences in the lungs, heart or liver from mutant and control mice. However, brain tissue exhibited multiple small hemorrhages in approximately 75% of mice lacking endothelial *Usp8*, whereas no hemorrhages were observed in control mice (Fig. 3b–d). Brain sections stained with hematoxylin and eosin (H&E) revealed that these hemorrhages were not localized to a specific area of the brain, but could be readily observed in the cortex, the striatum and the cerebellum among other areas (Fig. 3e–j). We further explored if Usp8$^{i\Delta EC}$ mice also presented higher vessel permeability, in addition to the observed hemorrhages, by injecting mice with Evans Blue dye prior to brain harvest. Brains from mice with endothelial loss of *Usp8* displayed higher Evans Blue extravasation compared to control mice (Supplementary Fig. 4).

Brain vascular structure was evaluated by whole-mount immunostaining a thick slice of the surface of the brain with anti-CD31 and anti-endomucin. Vascular density remained comparable between mutant and control mice; however, reduced branching frequency and increased luminal diameters across all vascular segments —including arteries, veins, and capillaries— was observed (Fig. 3k–o). Consistent with these observations, immunostaining of sagittal sections of

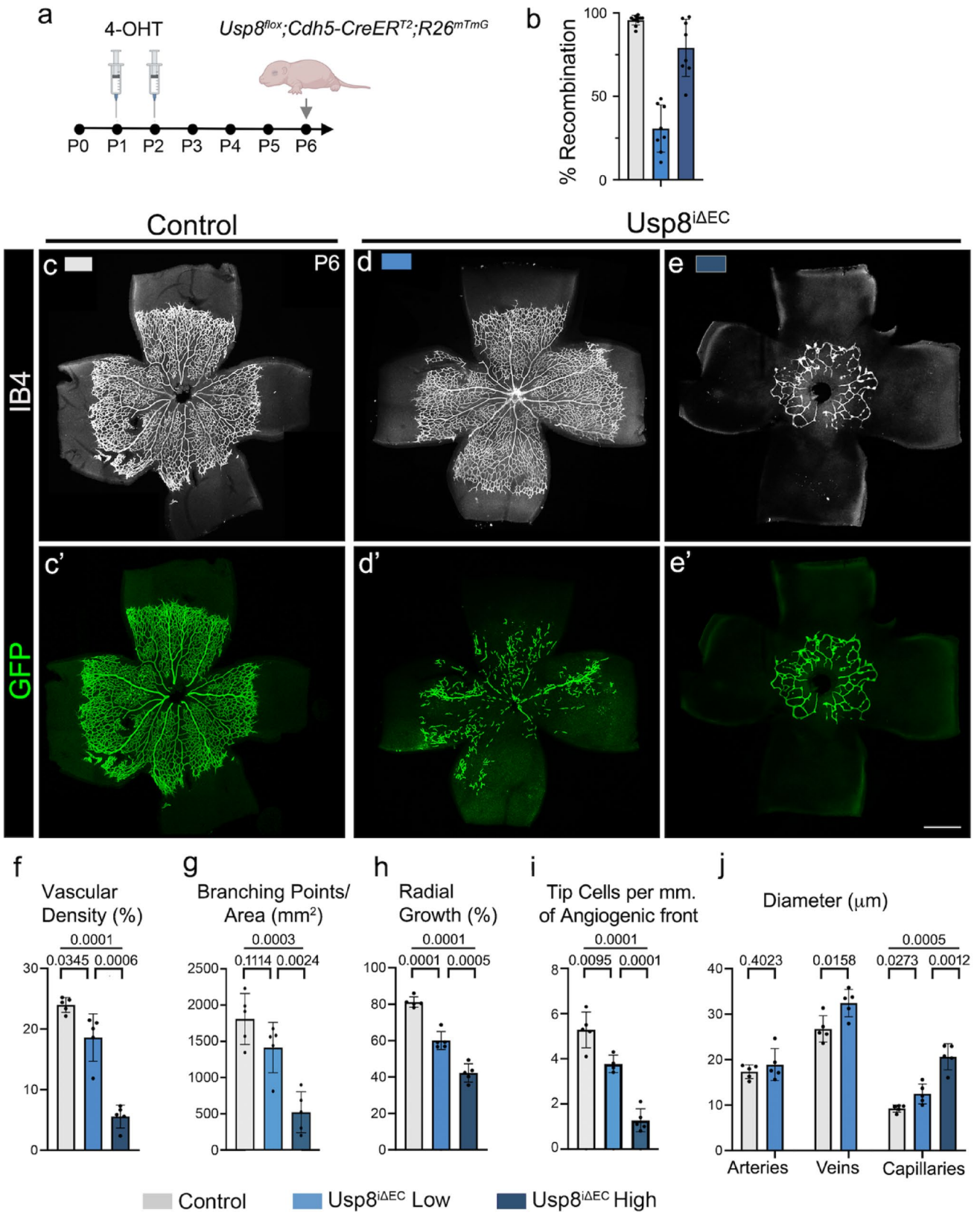
a
4-OHT
Usp8flox;Cdh5-CreERT2;R26mTmG
P0 P1 P2 P3 P4 P5 P6
b
% Recombination
100
50
0
Control
Usp8iΔEC
IB4
GFP
c P6
d
e
c'
d'
e'
f
Vascular Density (%)
0.0001
0.0345 0.0006
g
Branching Points/ Area (mm²)
0.0003
0.1114 0.0024
h
Radial Growth (%)
0.0001
0.0001 0.0005
i
Tip Cells per mm. of Angiogenic front
0.0001
0.0095 0.0001
j
Diameter (μm)
0.4023
0.0158
0.0005
0.0273 0.0012
Arteries
Veins
Capillaries
Control
Usp8iΔEC Low
Usp8iΔEC High

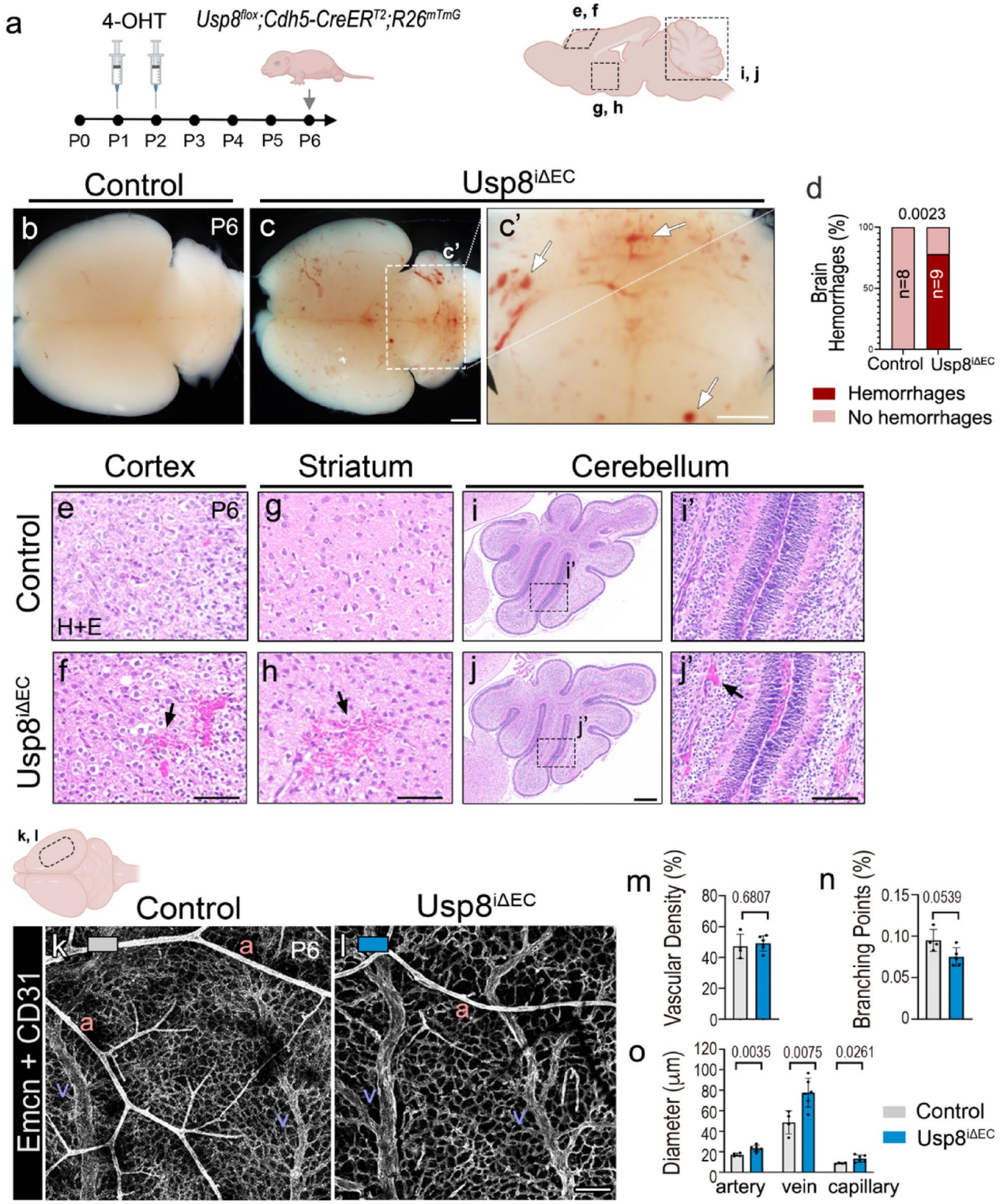

the whole brain similarly revealed increased perimeter of the vascular lumen in all areas of the brain and no differences in endothelial cell density (Supplementary Fig. 3a–i).

We also evaluated brain tissue to determine whether *Usp8* was being depleted after tamoxifen treatment of Usp8$^{i\Delta EC}$ mice. We used RNAscope probes recognizing *Usp8* and *Pecam* and observed a mosaic pattern of expression of *Usp8*

Fig. 3 Endothelial USP8 is essential for brain vascular integrity. **a** Left, experimental design; right, schematic representation of a brain's sagittal section with boxed areas depicting the regions analyzed in e–j. **b**, **c** Representative images of whole brains from control and Usp$^{i\Delta EC}$ P6 mice. Arrows in c' point to hemorrhages. **d** Quantification of brain hemorrhages. Data were analyzed using Fisher's exact test. **e–j** Representative images from H&E staining of **e**, **f** cortex, **g**, **h** striatum and **i**, **j** cerebellum sections of control and Usp$^{i\Delta EC}$ P6 mice. **i'**, **j'** Higher magnification images from boxed areas in i, j. Arrows point to accumulations of red blood cells. **k**, **l** Whole-mount brain immunofluorescent labeling with anti-Endomucin (Emcn, gray) and anti-CD31 (gray) of control and Usp$^{i\Delta EC}$ P6 brain cortex slices. a = arteries; v = veins. **m–o** Quantification of vascular density (**m**), branching points (**n**), and diameter of arteries, veins, and capillaries (**o**) of P6 control and Usp$^{i\Delta EC}$ whole-mount cortex slices ($n \geq 4$ slices per genotype). Bars represent mean ± S.D except for (**d**). Data were analyzed using unpaired T-test with Welch's correction except when stated otherwise. Scale bars indicate 1 mm in b–c', 100 µm in e–h, 200 µm in i–j and 100 µm in f–i

in the vasculature. Nonetheless, we could detect several abnormal vessel areas lacking *Usp8* signal compared to control mice (Supplementary Fig. 5) indicative of vascular depletion of *Usp8* in our mutant mice.

Next, we evaluated the vasculature of the lungs, heart and liver by immunostaining paraffin sections with anti-endomucin and anti-ERG to label the blood vessels and endothelial cell nuclei, respectively. No significant differences were observed in the endothelial cell density of lungs or liver between Usp8$^{i\Delta EC}$ and control mice (Supplementary Fig. 3j–m, t–w), however a small decrease in endothelial cell density was detected in the heart of Usp8$^{i\Delta EC}$ mice compared to control (Supplementary Fig. 3n–s).

Taken together our results suggest an organ-dependent role for endothelial USP8, playing a key role in the postnatal brain vasculature, but with milder effects on the postnatal heart's vasculature, and no differences in lung or liver endothelial density.

Partial recombination of endothelial *Usp8* can be compensated by non-recombined endothelial population

To explore the potential long-term consequences of the loss of endothelial *Usp8* after birth, tamoxifen-treated Usp8$^{i\Delta EC}$ and control mice carrying the *R26*$^{mT/mG}$ allele were allowed to reach adulthood and their tissues were evaluated at 12 weeks of age (Supplementary Fig. 6a). Analysis of survival of Usp8$^{i\Delta EC}$ mice revealed that the majority (75%) of mutant mice survived to adulthood (Supplementary Fig. 6b). Whole-mount analysis of the retinal vasculature did not show any differences in vascular density or branching points between mutant and control mice (Supplementary Fig. 6c–f). Similarly, we detected no differences in the diameter of arteries, capillaries, or veins (Supplementary Fig. 6g) between mice with endothelial loss of *Usp8* and control mice. Tissue analysis of survivors showed that, contrary to what was observed in early postnatal analysis, no hemorrhages were present in the brain parenchyma of surviving mutant mice at 12 weeks of age (Supplementary Fig. 6h, i). Notably, most endothelial cells (70%) in mutant mice that reached adulthood lacked mGFP signal from the *R26*$^{mT/mG}$ allele (Supplementary Fig. 6j), suggesting these cells may not have undergone *Usp8* deletion and thus might have a competitive advantage during angiogenesis and vascular maturation.

Overall, our data suggest that mosaic deletion of *Usp8* in endothelial cells results in impaired cellular functions during development which in many cases can be compensated/outcompeted by wild-type cells and result in a normal vascular development.

Adult deletion of endothelial *Usp8* does not reveal overt vascular anomalies

Next, we aimed to investigate whether endothelial USP8 plays a role in vessel homeostasis in addition to its function in angiogenesis. For this purpose, we induced *Usp8* gene deletion in adulthood by delivering tamoxifen to 6-week-old Usp8$^{i\Delta EC}$ and control mice. We analyzed the vasculature of different tissues eight weeks later (Supplementary Fig. 7a).

Analysis of the whole-mount retina immunolabeled with IsolectinB4 to highlight the blood vessels showed around 90% recombination of the *R26*$^{mT/mG}$ allele in Usp8$^{i\Delta EC}$ mice pointing to an efficient deletion of endothelial *Usp8* in these mice (Supplementary Fig. 7b, d). Evaluation of the vascular plexus revealed no differences in the vascular density or in the number of branching points of Usp8$^{i\Delta EC}$ compared to control mice (Supplementary Fig. 7c–f). Similarly, no differences were observed in the diameter of the arteries, capillaries, or veins between mutant and control mice (Supplementary Fig. 7g). Examination of the whole brain after dissection did not reveal any hemorrhage in mutant or control mice (Supplementary Fig. 7h). To determine whether deeper microhemorrhages might be present in the brain that could not be detected by gross evaluation, we stained paraffin sections with H&E. Our analysis showed that there were no detectable hemorrhages in the brain tissue of mice with endothelial loss of *Usp8* (Supplementary Fig. 7i–j).

Immunohistochemical analysis using IsolectinB4, anti-endomucin, and anti-ERG in paraffin sections from brain, lung, heart, and liver of Usp8$^{i\Delta EC}$ and control mice did not reveal any differences in the vessel or endothelial cell density of these tissues (Supplementary Fig. 8). The lack of vascular anomalies prompted us to verify whether *Usp8* expression was also present in adult tissue. We labeled brain sections with RNAscope probes targeting *Pecam*, *Acta2*, and *Usp8*. Our analysis revealed low levels of Usp8 expression, with

no apparent differences across vascular segments (Supplementary Fig. 1b), indicating that the absence of a vascular response was not due to a lack of Usp8 expression.

In summary, loss of endothelial *Usp8* in adult mice indicates that USP8 is not crucial for vessel maintenance and homeostasis.

USP8 regulates endothelial cell-cycle activation

To further understand how USP8 modulates endothelial cell biology and alters the angiogenic response, we evaluated endothelial cell proliferation, a key driver of angiogenesis. We first determined whether there were differences in endothelial proliferation at E9.5 between *Usp8*^{flox}; *Tie2Cre* and control embryos. For this purpose, we injected 5-ethynyl-2′-deoxyuridine (EdU) and analyzed the degree of endothelial cell EdU incorporation in the DA, CV and the MV. Our data showed a small, though not significant reduction in endothelial proliferation in the CV and MV, but no differences in the DA (Fig. 4a–c).

Next, we evaluated endothelial proliferation in the developing retina from P6 Usp8$^{i\Delta EC}$ and control mice. In this case, retinas were whole-mount immunostained with anti-Ki67 to identify nuclei of cells in cell-cycle, anti-ERG to label endothelial cells nuclei, and with IsolectinB4 to highlight the endothelium. Our analysis revealed a significant decrease in Ki67^{+} endothelial cells (a surrogate for proliferation) in the case of mutants exhibiting lower recombination, which was more pronounced in the group of mutants with a high level of recombination (Fig. 4d–h). Of note, we observed that in the group of mutants with low recombination, around 75% of the endothelial cells in cell-cycle (Ki67^{+}, ERG^{+}) were GFP-negative indicating that most of the proliferation was occurring in cells that most likely had not lost *Usp8* (Fig. 4i, j). Taken together, our data point to a key role for endothelial USP8 in regulating cell proliferation in the angiogenic postnatal retina.

Loss of endothelial USP8 leads to a higher cell number in enlarged vessels

Our findings of a greater vessel diameter in mice lacking endothelial *Usp8*, together with observations of reduced number of cells in cell-cycle, led us to question the reason for this discrepancy—specifically, whether the number or size of endothelial cells was altered in the capillaries and veins of Usp8$^{i\Delta EC}$ mice compared to controls. Alternatively, we also considered the possibility of cardiac malformations that could result in enlarged vessel diameters as a secondary effect.

When evaluated for malformations, heart sections from P6 Usp8$^{i\Delta EC}$ mice displayed no overt differences when compared with their control counterparts. Moreover, no significant differences were observed in the thickness of the septum or the left ventricular posterior wall (Supplementary Fig. 9) indicating that cardiac malformations were not present in mice with loss of endothelial *Usp8*.

To study if there were changes in endothelial cell size after the loss of endothelial *Usp8*, we immunostained whole mount P6 retina from Usp8$^{i\Delta EC}$ and control mice with anti-Vascular Endothelial Cadherin (VE-Cadherin or Cadherin 5). VE-Cadherin localizes to the endothelial cell membrane allowing for easy visualization and

measurement of cell shape. Our analysis revealed no differences in the endothelial surface area between mutant and control mice in arteries, capillaries or veins (Supplementary Fig. 10a–g).

We further evaluated whether endothelial cell number was altered in mutant mice compared to control. We quantified the number of endothelial cell nuclei (ERG^{+}) per vessel area. Our data showed a similar density of cells between Usp8$^{i\Delta EC}$ and control mice (Supplementary Fig. 10h). However, considering that vessel size of the mutants in the case of capillaries and veins, a similar cellular density implies a higher number of cells in these vessels.

We then questioned if the higher number of cells in mutant mice was a result of changes in susceptibility to apoptotic stimuli. To answer this, we immunostained wholemount P6

Fig. 4 Endothelial Usp8 loss leads to reduced cell-cycle entry. **a**, **b** Immunofluorescence of transverse sections from control and UspΔEC E9.5 embryos stained with anti-Bromodeoxyuridine (BrdU, green), IsolectinB4 (IsoB4, gray), and DAPI (blue). Yellow arrows indicate the cardinal vein, yellow arrowheads mark the dorsal aorta, and gray arrows point to the meningeal vessels. **c** Quantification of BrdU incorporation in endothelial cells from E9.5 control and UspΔEC embryos (n = 3 embryos per genotype). d.a.=dorsal aorta, c.v.=cardinal vein, m.v.=meningeal vessels. Bars represent mean ± S.D. Data were analyzed using unpaired T-test with Welch's correction. **d**–**f** Whole-mount P6 retinas from control and UspiΔEC mice immunolabeled with anti-Ki67 (green) and IsolectinB4 (IsoB4, blue). Boxed regions are magnified in **d'**–**f'**. Yellow arrows point to Ki67+ endothelial cells. **g** Top, quantification of the percentage of total Ki67+ endothelial cells in P6 control and UspiΔEC retinas (n ≥ 3 retinas per genotype). Bottom, quantification of Ki67+ endothelial cells in arteries, veins and capillaries. Bars represent mean ± S.D. Data were analyzed using unpaired T-test with Welch's correction. **h** Quantification of the number of endothelial cells in P6 control and UspiΔEC retinas (n ≥ 3 retinas per genotype). Data are represented using a violin plot. **i** Whole-mount P6 retina from UspΔEC mice with low recombination immunolabeled with anti-Ki67 (cyan), anti-ERG (magenta) and endogenous mGFP (green). Yellow arrows point to double Ki67+ and ERG+ cells. **j** Quantification of combined Ki67+ and GFP+ or Ki67+ GFP− cells in control, low and high recombined UspiΔEC retinas. Data represent percentage of proliferative mGFP+ and mGFP− cells (n = 4 retinas per genotype). **k**–**m** Whole-mount P6 retinas from control and UspiΔEC mice immunolabeled with anti-cleaved Caspase 3 (red), Isolectin B4 (IB4, blue) and ERG (gray). **n** Quantification of the percentage of cleaved Caspase 3 + endothelial cells in P6 control and UspiΔEC retinas (n ≥ 3 retinas per genotype). Boxed regions are magnified below. Scale bars indicate 25 μm in a–b, 250 μm in d–f and 50 μm in d'–f' and h

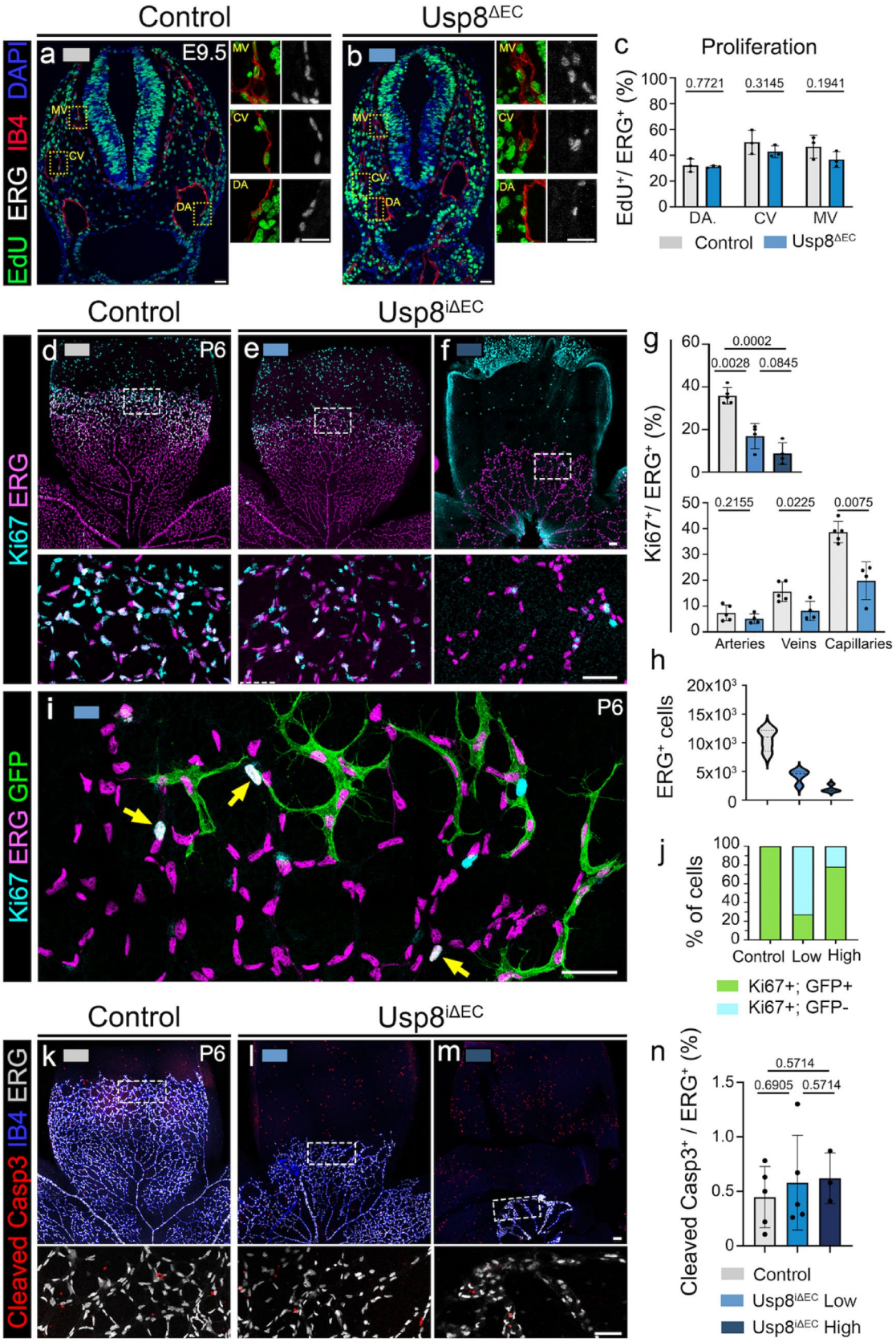
Control
Usp8ΔEC
EdU ERG IB4 DAPI
a E9.5
b
MV
CV
DA
c Proliferation
EdU+/ ERG+ (%)
0.7721
0.3145
0.1941
DA.
CV
MV
Control
Usp8ΔEC
Control
Usp8iΔEC
Ki67 ERG
d P6
e
f
g
Ki67+/ ERG+ (%)
0.0002
0.0028
0.0845
0.2155
0.0225
0.0075
Arteries
Veins
Capillaries
h
ERG+ cells
20x10³
15x10³
10x10³
5x10³
0
Ki67 ERG GFP
i P6
j
% of cells
Control
Low
High
Ki67+; GFP+
Ki67+; GFP-
Control
Usp8iΔEC
Cleaved Casp3 IB4 ERG
k P6
l
m
n
Cleaved Casp3+ / ERG+ (%)
0.5714
0.6905
0.5714
Control
Usp8iΔEC Low
Usp8iΔEC High

retinas from Usp8$^{i\Delta EC}$ and control mice with anti-Cleaved Caspase 3. We observed no differences in the percentage of endothelial cells expressing Cleaved Caspase 3 between mutant and control mice suggesting that loss of endothelial *Usp8* does not result in changes in endothelial cell apoptosis (Fig. 4k–n).

Taken together, this data indicates that *Usp8* does not regulate endothelial cell size or apoptosis. However, loss of *Usp8* in the endothelium results in an increased number of cells per vessel in mutant mice implying that Usp8$^{i\Delta EC}$ mice likely exhibit defects in endothelial cell migration.

Notch signaling in endothelial cells is not regulated by Usp8

The Notch signaling pathway plays key roles in endothelial cells during angiogenesis and arteriovenous specification [17]. Notch receptors in the cell surface interact with ligands in neighboring cells; this interaction triggers the cleavage of the protein releasing its intracellular domain (NICD) that translocates to the nucleus and promotes the transcription of its target genes. Previous works have described a role for USP8 promoting the stability of NICD and therefore modulating its signaling [18, 19]. To test whether Usp8 was regulating endothelial cell functions by altering Notch signaling we immunostained sections from E9.5 Usp8$^{\Delta EC}$ embryos and Control mice with anti-N1ICD. We evaluated N1ICD expression in the DA, CV and MVs and detected no significant differences between mutant and control mice (Supplementary Fig. 11). This data suggests that USP8 does not regulate endothelial cell functions by modulating the Notch signaling pathway.

The distribution and activation of VEGFR2 are altered in endothelial USP8-deficient mutants

VEGF-A acting through the VEGFR2 is the most relevant signaling axis in the angiogenic response [2]. Previous work in vitro has described a role for USP8 in regulating VEGFR2 trafficking and activation in human umbilical vein endothelial cells (HUVECs) [12]. Hence, we hypothesized that the abnormal angiogenic responses observed in mice lacking endothelial *Usp8* might result from impaired localization and activation of VEGFR2.

To evaluate whether loss of endothelial *Usp8* was altering the trafficking of VEGFR2, we immunostained sections from E9.5 *Usp8$^{flox/flox}$;Tie2^{Cre}* and control embryos with anti-VEGFR2 antibody. No differences were observed in the pattern of expression of VEGFR2 in the DA, however, in CV and MV of mutant embryos, VEGFR2 was mainly localized in enlarged intracellular vesicles (Fig. 5a–f). Double immunostaining of VEGFR2 and early endosome marker 1 (EEA1) revealed that VEGFR2 distribution in mutants was fundamentally aggregating in the endosomal compartment (Fig. 5k–n). We also studied the distribution of VEGFR2 in the retinal vasculature of P6 Usp8$^{i\Delta EC}$ and control mice. Consistent with our observations in the embryonic vasculature, we detected an abnormal distribution of VEGFR2 located in structures compatible with intracellular vesicles in the vessels from Usp8$^{i\Delta EC}$ mice which was not observed in the retinal vasculature from control mice (Fig. 5g–h). These data indicate that USP8 plays a critical role in regulating VEGFR2 intracellular trafficking in vivo.

Activation and signaling of VEGFR2 depend on its interaction with different partners, the timing of its presence in the plasma membrane and the rate of internalization and degradation [7, 20]. To gain further insights into the regulation of VEGFR2 and its plasma membrane-associated levels, we performed immunostaining for the receptor in non-permeabilizing conditions. Signal corresponding to VEGFR2 was evaluated together with signal from IsolectinB4 which labels de endothelial cell membrane. Our data show that intensity levels of VEGFR2 in the plasma membrane of endothelial cells from Usp8$^{i\Delta EC}$ mice were markedly lower than those of the control counterparts (Fig. 5i–j). Loss of membrane-bound levels of VEGFR2 are indicative of deficient availability to bind ligand and signal in Usp8$^{i\Delta EC}$ mice compared to control.

Fig. 5 Endothelial USP8 regulates VEGFR2 trafficking. **a–f** Immunofluorescence staining of E9.5 control and Usp$^{\Delta EC}$ embryonic transverse thoracic sections with anti-VEGFR2 (magenta) and DAPI (blue) showing the dorsal aorta (**a**, **b**; DA), the cardinal vein (**c**, **d**; CV) and meningeal vessels (**e**, **f**; MV). Arrows point to aggregated VEGFR2. **g–j'** Whole-mount P6 retinas from control and Usp$^{i\Delta EC}$ mice immunolabeled with anti-VEGFR2 (cyan), IsolectinB4 (IB4; magenta) and ERG (gray) in permeabilized (**g**, **h**) and non-permeabilized (**i**, **j**) retinas. Graph represents intensity of the RGB profile along the yellow arrows in I' and j'; yellow arrowheads point to the peak intensity of IB4 (blue) and VEGFR2 (red) in non-permeabilized retinas. **k**, **n'** Immunofluorescence staining of meningeal vessels of E9.5 control and Usp$^{\Delta EC}$ embryonic transversal thoracic sections stained with anti-VEGFR2 (red), anti-Early Endosome Antigen 1 (EEA-1; gray), and DAPI (blue). Boxed regions are magnified in **m'**,**n'**. Arrows point to VEGFR2 localization in early endosomes. **k–l'** Immunofluorescence staining of control and Usp$^{i\Delta EC}$ P6 whole-mount retinas with anti-VEGFR2 (red) and anti-ERG (gray). Arrows point to abnormal VEGFR2 aggregates. **o**, **p** Immunofluorescence staining of E9.5 control and Usp$^{\Delta EC}$ embryonic transversal thoracic sections with anti-phospho ERK (pERK; cyan), IsolectinB4 (IB4; red), and DAPI (blue). CV is cardinal vein, DA is dorsal aorta and MV are meningeal vessels. **q** Quantification of pERK in endothelial cells of transversal thoracic sections from E9.5 control and Usp$^{\Delta EC}$ embryos. **r–t** Whole-mount P6 retinas from control (white box) and Usp$^{i\Delta EC}$ mice with low (light blue box) or high (dark blue box) recombination immunolabeled with anti-pERK (pERK; cyan) and IsolectinB4 (IB4; red). **u** Quantification of pERK in endothelial cells from control (gray) and and Usp$^{i\Delta EC}$ P6 retinas with low (light blue) or high (dark blue) recombination ($n \geq 3$ retinas per genotype). Bars represent mean ± S.D. Data were analyzed using unpaired T-test with Welch's correction. Scale bars indicate 5 µm in a–f and k–n'; 20 µm in g–j', 25 µm in o–p and 100 µm in r–t

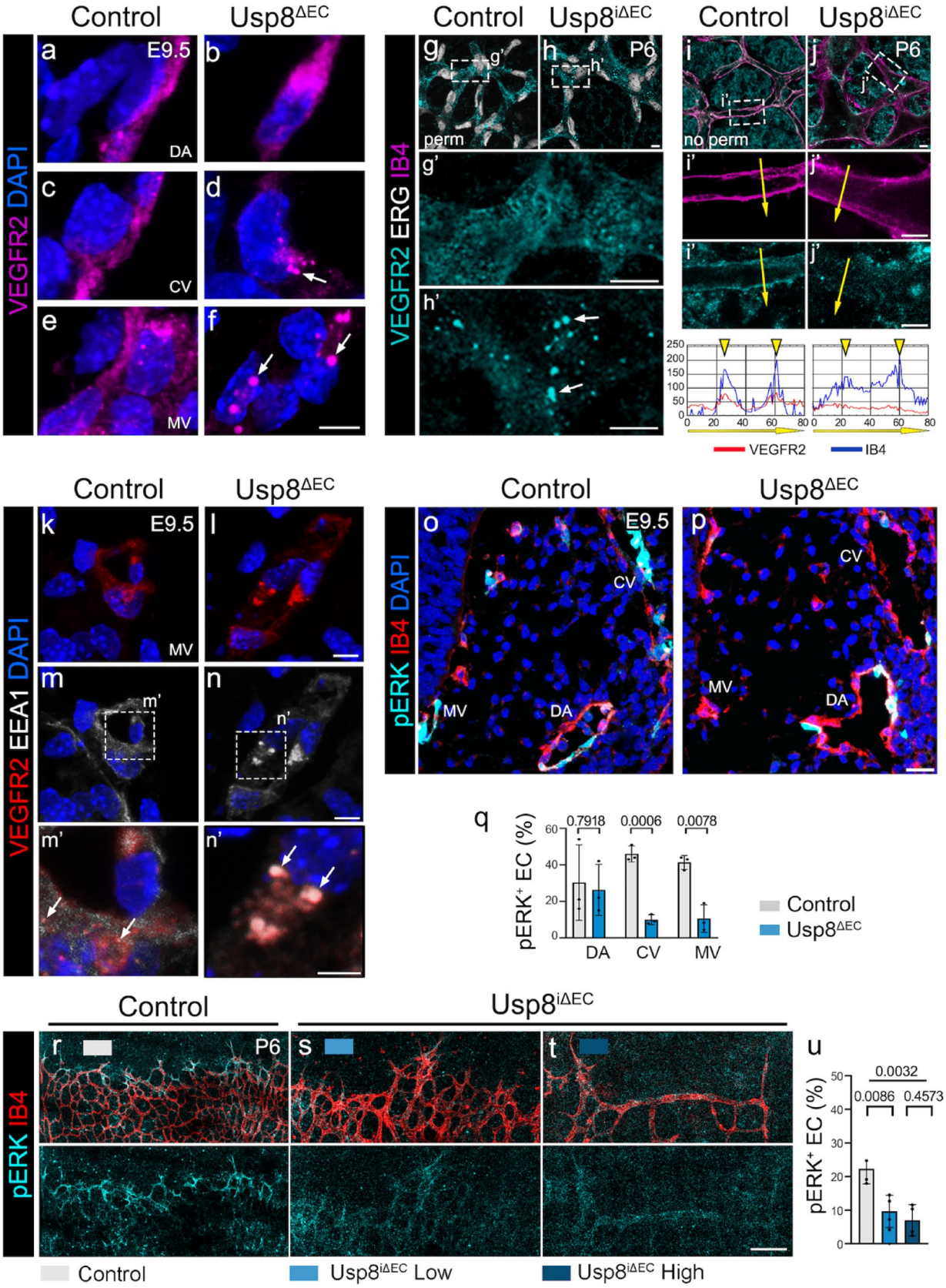
Control
Usp8ΔEC
Usp8iΔEC
VEGFR2 DAPI
VEGFR2 ERG IB4
VEGFR2 EEA1 DAPI
pERK IB4 DAPI
pERK IB4
E9.5
P6
DA
CV
MV
perm
no perm
VEGFR2
IB4
pERK+ EC (%)
0.7918
0.0006
0.0078
0.0032
0.0086
0.4573
Control
Usp8ΔEC
Usp8iΔEC Low
Usp8iΔEC High

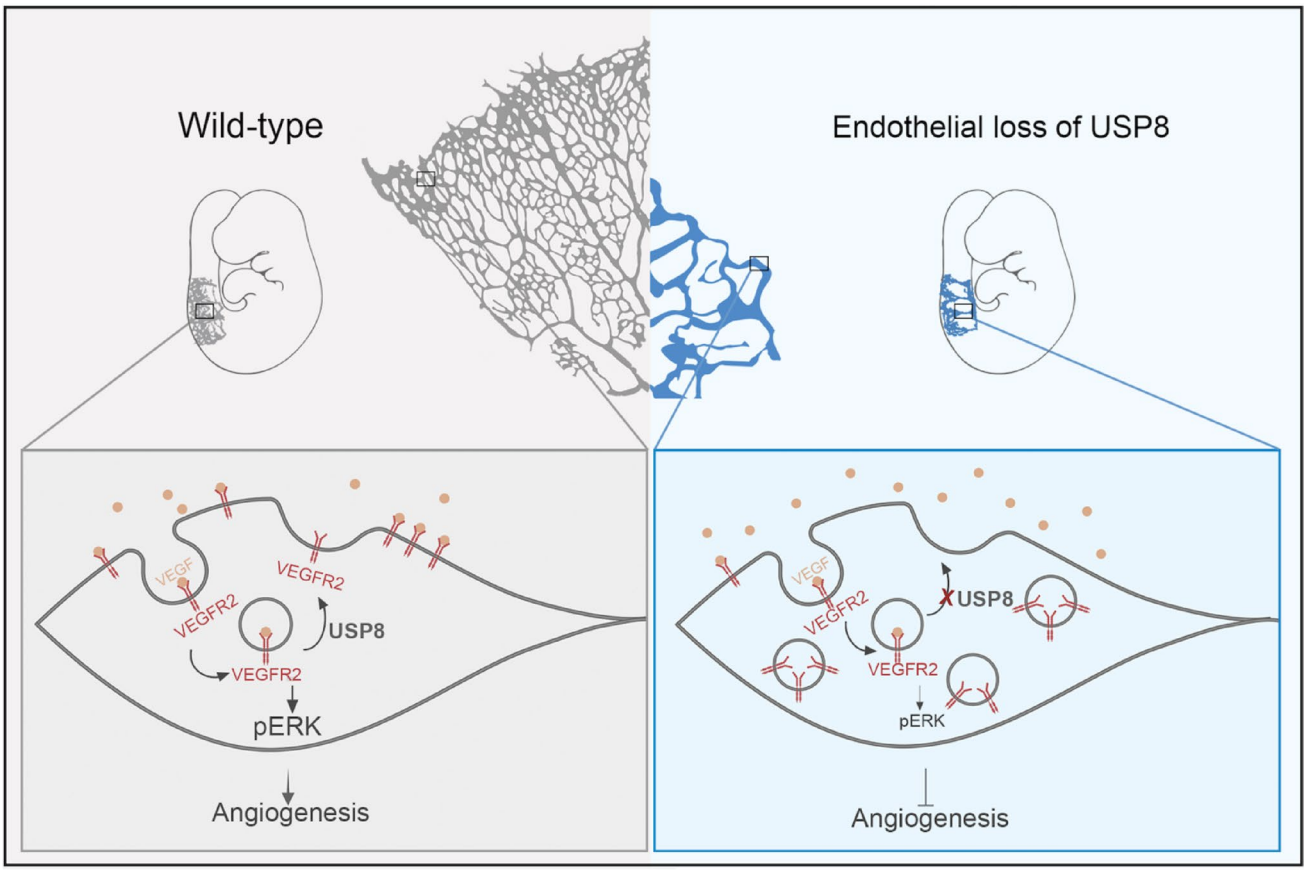

Fig. 6 Working model for endothelial USP8 function. Left panel: In wild-type embryonic vessels and angiogenic retina, USP8 regulates VEGFR2 trafficking, ensuring its activation and recycling to the membrane, enabling adequate angiogenic response. Right panel: In mice with endothelial *Usp8* loss, VEGFR2 trafficking is disrupted, preventing its degradation and/or recycling to the membrane. This leads to reduced VEGFR activation, decreased pERK signaling, and impaired angiogenesis

Our previous data showing a deficient angiogenic response in mice with loss of endothelial *Usp8*, together with the observed abnormal trafficking of the receptor led us to investigate whether VEGFR2 activation was reduced in our mutant mice. For this purpose, we evaluated the levels of pERK in endothelial cells as an indicator of VEGFR2 activation [4]. Anti-pERK immunostaining of sections from $Usp8^{flox/flox};Tie2^{Cre}$ and control embryos demonstrated a marked reduction in endothelial pERK levels in the CV and MV, with no reduction observed in the DA (Fig. 5o–q). Similarly, analysis of pERK in the postnatal retinal vasculature of $Usp8^{i\Delta EC}$ and control P6 mice revealed a significant decrease in endothelial pERK in mutant mice with low recombination, with an even more pronounced reduction in mutants with high recombination (Fig. 5r–u). Altogether, our data indicate that USP8 is essential for regulating VEGFR2 trafficking and activation in vivo, leading to lower ERK activation.

Discussion

Angiogenesis, the generation of new blood vessels from preexisting ones, is essential during development and plays key roles in many pathological conditions [2]. Here, we show, for the first time, that the deubiquitinase USP8 plays critical roles during angiogenesis. Endothelial *Usp8* deletion impaired angiogenesis during embryonic and postnatal stages but did not affect endothelial cell homeostasis in adulthood. Mechanistically, we describe how the loss of endothelial *Usp8* disrupts VEGFR2 trafficking, leading to its accumulation in intracellular vesicles, which, in turn, reduces pERK signaling and endothelial cell-cycle activation (Fig. 6). Altogether, our work has identified endothelial USP8 as a key regulator of angiogenesis, and an attractive potential target for antiangiogenic therapies.

Our data show that loss of endothelial *Usp8* during embryonic development results in embryonic lethality by E10.5. Embryonic vascular development begins around E7.5 with the specification and formation of the first set of vessels from endothelial progenitors. Next, the vascular

plexus develops through angiogenesis and continues deploying until around E11.5, when vessels mature. Mice with loss of most of the well-known angiogenesis regulators exhibit embryonic lethality at these early stages of vessel formation [21]. In the case of VEGFR2, embryos with full loss of the gene (*Flk1*) die *in utero* between E8.5 and E9.5 showing profound defects in vascular development [22]. We believe that our findings of impaired angiogenesis in the intersomitic vessels and abnormal vasculature in E9.5 $Usp8^{\Delta EC}$ embryos, along with embryonic lethality by E10.5, support a critical role for endothelial USP8 in developmental angiogenesis.

Analysis of the postnatal retinal vasculature, following the induced deletion of endothelial *Usp8*, revealed significant variability in recombination levels resulting in a genetic mosaic where wild-type and mutant endothelial cells coexist within the same tissue and microenvironment. We also observed that the differences in recombination associated with variations in the severity of the vascular phenotype. Considering our findings that loss of *Usp8* impairs VEGFR2 signaling and renders endothelial cells less capable of forming new vessels, we propose a model where, in mosaic recombination with low efficiency, non-recombined (wild-type) cells would out-compete cells lacking *Usp8.* This situation would lead to a mild angiogenic phenotype, as wild-type cells take over the vasculature, allowing it to develop and function adequately.

When recombination is highly efficient, the few remaining wild-type cells cannot compensate for the impaired mutant cells, resulting in defective angiogenesis and a severe phenotype. Consistent with this, when mice were allowed to reach adulthood after postnatal induction of *Usp8* recombination, survival was arrested in approximately 25% of them. This likely reflects the subset of mice that underwent efficient *Usp8* recombination, where the resulting severe angiogenic phenotype proved lethal. In contrast, with partial recombination, wild-type cells in the vasculature could gradually compensate for *Usp8* loss, maintain function, and enable survival into adulthood without an overt phenotype.

Consistent with our findings, Zarkada et al. [23] describe how variable *Flk1* deletion efficiency in endothelial cells leads to different retinal angiogenesis phenotypes due to the competitive advantage of non-recombined cells. Garcia-González et al. [24] took this further by using the iSuRe-HadCre mouse strain, which enhances Cre-recombinase potency and labels recombined cells with TdTomato. This tool enabled them to generate and visualize mosaic or full *Flk1* recombination. Their observations on how differential Flk1 recombination affects retinal angiogenesis align with those of Zarkada et al. and, importantly, phenocopy the retinal vascular defects observed in our models with high and low efficiencies of postnatal endothelial *Usp8* deletion. These findings reinforce our conclusion that endothelial USP8 loss impairs angiogenesis by regulating VEGFR2 activity.

Postnatal endothelial loss of Usp8 affected the vasculature of the brain and heart but not the liver or lungs. Similarly, *Flk1* deletion reduced vascular density in the retina, liver, and heart, though its effects on the brain and lungs were not assessed [25]. Our findings largely align with those for *Flk1*, except in the liver, where endothelial *Usp8* loss had no apparent impact. This discrepancy may stem from insufficient recombination efficiency in certain tissues (liver and lung), though a distinct role for USP8 in different vascular beds cannot be ruled out.

Because endothelial *Usp8* loss mimics VEGFR2 deficiency, and *Flk1* deletion impairs angiogenesis with widespread vascular density reductions, similar effects may be expected in the brain. However, our data show that endothelial *Usp8* loss does not significantly alter brain vascular density but instead leads to vessel enlargement, increased permeability, and microhemorrhages across all analyzed regions. Increased permeability and vessel dilation are often responses to elevated VEGFA signaling [26] which seems contradictory to the proposed reduction in VEGFR2 signaling. The underlying mechanism responsible for the observed vascular abnormalities in the brain remains to be determined. However, we propose a model in which loss of VEGFR2 expression in the membrane of endothelial cells results in an excess of available VEGFA. This surplus of VEGFA may overstimulate the VEGFR2 receptor in non-recombined wild-type cells, promoting vessel leakage. In parallel, dilated vessels containing *Usp8*-deficient cells might be more prone to rupture resulting in the observed microhemorrhages.

Our analysis of the postnatal retinal vasculature after endothelial *Usp8* loss revealed a significant reduction in endothelial cell cell-cycle entry, consistent with a role for USP8 in regulating VEGFR2 trafficking. However, examination of the embryonic vasculature showed no significant differences in the vascular segments evaluated. While retinal angiogenesis is well-characterized, with defined stages as sprouting, vessel elongation, arteriovenous specification, remodeling and maturation, embryonic vascular development is more complex and less temporally uniform. Although we observed angiogenic differences in intersomitic vessels, the vascular segments analyzed for proliferation at E9.5 (DA, CV and MVs) may have already started entered maturation and arrested proliferation, potentially obscuring the impact of *Usp8* loss on endothelial proliferation in these contexts.

In both the angiogenic embryo and postnatal retina, we observed a significant enlargement of venous and capillary segments diameter, while the arterial compartment remained unaffected. The remodeling of the immature

capillary plexus into distinct arterial, venous, or capillary fates relies on endothelial cell migration from venous/capillary segments towards arteries [27–29], a process regulated by VEGF-VEGFR2 signaling and shear stress [30]. We propose that endothelial *Usp8* loss, which disrupts VEGFR2 trafficking, impairs VEGFR2 signaling during this remodeling phase. As a result, endothelial cell migration toward arteries is compromised, leading to an accumulation of endothelial cells within capillaries and veins. This "entrapment" likely accounts for the observed vessel enlargement in these compartments.

Overall, arteries in our study appear refractory to *Usp8* loss. Unlike capillaries and veins, arterial endothelial cells in mutant embryos do not exhibit mislocalized VEGFR2 aggregates in enlarged vesicles, nor do they show reduced pERK levels. One possible explanation, given the mosaic recombination, is that non-recombined cells preferentially populate the arteries. As noted earlier, recombined cells with lower VEGFR2 activity may be unable to migrate towards arteries, leading to their selective enrichment with wild-type endothelial cells. Alternatively, redundancy within the deubiquitinating enzyme family could compensate for USP8 loss in arteries. While multiple USP family members are expressed in endothelial cells, their vascular segment-specific expression patterns and roles in angiogenesis remain poorly defined [31–43]. Further studies are needed to clarify these mechanisms and the function of deubiquitinases in vascular development.

Our work has primarily focused on VEGFR2 regulation by USP8 as the main driver of vascular phenotypes in $Usp8^{i\Delta EC}$ mice. However, we cannot exclude the possibility that USP8 also modulates other key regulators of angiogenesis. Both VEGFR1 and VEGFR3 play important roles in vascular development and, like VEGFR2, are subject to ubiquitination and trafficking-dependent activation [1, 44, 45]. The chemokine receptor CXCR4, an essential mediator of angiogenic sprouting [46], has been reported to be regulated by USP8 in other cell types [47]. Interestingly, USP8 loss in those contexts results in increased CXCR4 surface levels and enhanced ERK phosphorylation, which contrasts with our observations in $Usp8^{i\Delta EC}$ mice. Moreover, the Frizzled-4 receptor (FZD4), a key regulator of angiogenesis and vascular permeability [48], is controlled by intracellular trafficking [49] and interacts with USP8 [50]. Importantly, loss-of-function phenotypes of these regulators do not mimic the vascular defects seen in our mutants. Thus, VEGFR2 dysregulation likely accounts for the predominant effects, with additional USP8 targets contributing more subtly.

Our studies identify endothelial USP8 as a key regulator in angiogenesis, yet its absence does not disrupt endothelial homeostasis, making it a promising target for anti-angiogenic therapies. Pathological neo-angiogenesis underlies numerous diseases, including cancer and ocular diseases [51]. While anti-angiogenic tumor therapies face challenges such as resistance, combining them with chemotherapy or immunotherapy, has shown promise [52]. The USP8-specific inhibitor DUBS-in2 [53] exhibits strong anti-tumor potential by targeting the immunological tumor microenvironment [54, 55], positioning USP8 as a potential co-therapeutic target in cancer treatment.

In neovascular eye diseases like age-related macular degeneration, diabetic retinopathy, and retinopathy of prematurity, VEGF-targeting therapies are clinically effective, but a subset of patients develop resistance after prolonged treatment [56]. This underscores the need for alternative strategies. Further studies will determine whether USP8 inhibitors, such as DUBS-in2, could offer viable therapeutic or co-therapeutic options for neovascular eye diseases.

Supplementary Information The online version contains supplementary material available at https://doi.org/10.1007/s10456-025-10027-3.

Acknowledgements We would like to thank Dr. Klaus-Peter Knobeloch for kindly providing the $Usp8^{flox}$ mouse line, Abel Galicia Martín and Lucia Méndez Peralta for their help with animal husbandry, and the CNIC Comparative Medicine and Microscope facilities for their support. We are also grateful for the support received by Dr. Mariona Graupera during the completion of this project.

Author contributions H.C., J.G.-B. and J.L.P. designed the experiments; A.P-N., M.L.L., A.A.U, and T.G.-C. performed the experimental work; H.C., A.P-N. J. G.-B. analyzed the data; H.C. and J. G.-B. drafted the manuscript; J.L.P. obtained funding, reviewed and edited the manuscript. All authors have reviewed and approved the final version submitted for publication.

Funding This work was supported by grants PID2022-136942OB-I00 and CB16/11/00399 (CIBER CV) from MICIU/AEI/https://doi.org/10.13039/501100011033 and by ERDF/EU, and a grant for Research in Familial Cardiomyopathies and Cardiovascular Genetics (SECSCFG-INV-CFG 21) from the Spanish Society of Cardiology to J.L.d.l.P.; 2020–5 A/BMD-19729 mod.1 grant funded by "Atracción de Talento Investigador" Call from CAM to J. G.-B.; 2020-T1/BMD-19985 mod.1 grant funded by "Atracción de Talento Investigador" call from CAM and PID2022-137473OB-I00 from MICIU to H.C. A.P-N was supported by a PhD contract from MICIU/AEI /https://doi.org/10.13039/501100011033 and FSE+ (ref. PRE2022-102314); T.G-C. was supported by a PhD contract from MICIU (ref. FPU18/01054); M.L.L. was awarded a 2021 CNIC Cicerone training fellowship. The CNIC is supported by the Instituto de Salud Carlos III (ISCIII), the MCIU, and the Pro CNIC Foundation, and is a Severo Ochoa Center of Excellence (grant CEX2020-001041-S funded by MICIU/AEI/https://doi.org/10.13039/501100011033). The CNIC microscope facility is funded by the ReDIB ICTS infrastructure TRIMA@CNIC from MCIN.

Data availability No datasets were generated or analysed during the current study.

Declarations

Competing interests The authors declare no competing interests.

Ethic approval Animal studies were approved by the CNIC Animal Experimentation Ethics Committee and by the Community of Madrid (Ref. PROEX 054.6/25). All animal procedures conformed to EU Directive 2010/63EU and Recommendation 2007/526/EC regarding the protection of animals used for experimental and other scientific purposes, enacted in Spanish law under Real Decreto 118/2021 (modification on Real Decreto 53/2013) and Ley 32/2007.

References

1. Furtado J, Eichmann A (2024) Vascular development, remodeling and maturation. Curr Top Dev Biol 159:344–370. https://doi.org/10.1016/bs.ctdb.2024.02.001
2. Eelen G, Treps L, Li X, Carmeliet P (2020) Basic and therapeutic aspects of angiogenesis updated. Circ Res 127(2):310–329. https://doi.org/10.1161/CIRCRESAHA.120.316851
3. BetsholtzC (2018) Cell-cell signaling in blood vessel development and function. EMBO Mol Med https://doi.org/10.15252/emmm.201708610
4. Simons M, Gordon E, Claesson-Welsh L (2016) Mechanisms and regulation of endothelial VEGF receptor signalling. Nat Rev Mol Cell Biol 17(10):611–625. https://doi.org/10.1038/nrm.2016.87
5. Koch S, Claesson-Welsh L (2012) Signal transduction by vascular endothelial growth factor receptors. Cold Spring Harb Perspect Med 2(7):a006502. https://doi.org/10.1101/cshperspect.a006502
6. Lampugnani MG, Orsenigo F, Gagliani MC, Tacchetti C, Dejana E (2006) Vascular endothelial Cadherin controls VEGFR-2 internalization and signaling from intracellular compartments. J Cell Biol 174(4):593–604. https://doi.org/10.1083/jcb.200602080
7. Nakayama M, Nakayama A, van Lessen M, Yamamoto H, Hoffmann S, Drexler HC, Itoh N, Hirose T, Breier G, Vestweber D, Cooper JA, Ohno S, Kaibuchi K, Adams RH (2013) Spatial regulation of VEGF receptor endocytosis in angiogenesis. Nat Cell Biol 15(3):249–260. https://doi.org/10.1038/ncb2679
8. Lanahan AA, Hermans K, Claes F, Kerley-Hamilton JS, Zhuang ZW, Giordano FJ, Carmeliet P, Simons M (2010) VEGF receptor 2 endocytic trafficking regulates arterial morphogenesis. Dev Cell 18(5):713–724. https://doi.org/10.1016/j.devcel.2010.02.016
9. Mevissen TET, Komander D (2017) Mechanisms of deubiquitinase specificity and regulation. Annu Rev Biochem 86:159–192. https://doi.org/10.1146/annurev-biochem-061516-044916
10. Clague MJ, Urbe S, Komander D (2019) Breaking the chains: deubiquitylating enzyme specificity begets function. Nat Rev Mol Cell Biol 20(6):338–352. https://doi.org/10.1038/s41580-019-0099-1
11. CritchleyWR, Pellet-Many C, Ringham-Terry B, Harrison MA, Zachary IC, Ponnambalam S (2018) Receptor tyrosine kinase ubiquitination and De-Ubiquitination in signal transduction and receptor trafficking. Cells https://doi.org/10.3390/cells7030022
12. Smith GA, Fearnley GW, Abdul-Zani I, Wheatcroft SB, Tomlinson DC, Harrison MA, Ponnambalam S (2016) VEGFR2 Trafficking, signaling and proteolysis is regulated by the ubiquitin isopeptidase USP8. Traffic 17(1):53–65. https://doi.org/10.1111/tra.12341
13. Niendorf S, Oksche A, Kisser A, Lohler J, Prinz M, Schorle H, Feller S, Lewitzky M, Horak I, Knobeloch KP (2007) Essential role of ubiquitin-specific protease 8 for receptor tyrosine kinase stability and endocytic trafficking in vivo. Mol Cell Biol 27(13):5029–5039. https://doi.org/10.1128/MCB.01566-06
14. Kisanuki YY, Hammer RE, Miyazaki J, Williams SC, Richardson JA, Yanagisawa M (2001) Tie2-Cre Transgenic mice: a new model for endothelial cell-lineage analysis in vivo. Dev Biol 230(2):230–242. https://doi.org/10.1006/dbio.2000.0106
15. Wang Y, Nakayama M, Pitulescu ME, Schmidt TS, Bochenek ML, Sakakibara A, Adams S, Davy A, Deutsch U, Luthi U, Barberis A, Benjamin LE, Makinen T, Nobes CD, Adams RH (2010) Ephrin-B2 controls VEGF-induced angiogenesis and lymphangiogenesis. Nature 465(7297):483–486. https://doi.org/10.1038/nature09002
16. Muzumdar MD, Tasic B, Miyamichi K, Li L, Luo L (2007) A global double-fluorescent Cre reporter mouse. Genesis 45(9):593–605. https://doi.org/10.1002/dvg.20335
17. Siebel C, Lendahl U (2017) Notch signaling in Development, tissue Homeostasis, and disease. Physiol Rev 97(4):1235–1294. https://doi.org/10.1152/physrev.00005.2017
18. Liu T, Zhang C, Ying J, Wang Y, Yan G, Zhou Y, Lu G (2023) Inhibition of the intracellular domain of Notch1 results in vascular endothelial cell dysfunction in sepsis. Front Immunol 14:1134556. https://doi.org/10.3389/fimmu.2023.1134556
19. Shin S, Kim K, Kim HR, Ylaya K, Do SI, Hewitt SM, Park HS, Roe JS, Chung JY, Song J (2020) Deubiquitylation and stabilization of Notch1 intracellular domain by ubiquitin-specific protease 8 enhance tumorigenesis in breast cancer. Cell Death Differ 27(4):1341–1354. https://doi.org/10.1038/s41418-019-0419-1
20. Simons M (2012) An inside view: VEGF receptor trafficking and signaling. Physiol (Bethesda) 27(4):213–222. https://doi.org/10.1152/physiol.00016.2012
21. Rossant J, Howard L (2002) Signaling pathways in vascular development. Annu Rev Cell Dev Biol 18:541–573. https://doi.org/10.1146/annurev.cellbio.18.012502.105825
22. Shalaby F, Rossant J, Yamaguchi TP, Gertsenstein M, Wu XF, Breitman ML, Schuh AC (1995) Failure of blood-island formation and vasculogenesis in Flk-1-deficient mice. Nature 376(6535):62–66. https://doi.org/10.1038/376062a0
23. Zarkada G, Heinolainen K, Makinen T, Kubota Y, Alitalo K (2015) VEGFR3 does not sustain retinal angiogenesis without VEGFR2. Proc Natl Acad Sci U S A 112(3):761–766. https://doi.org/10.1073/pnas.1423278112
24. Garcia-Gonzalez I, Rocha SF, Hamidi A, Garcia-Ortega L, Regano A, Sanchez-Munoz MS, Lytvyn M, Garcia-Cabero A, Roig-Soucase S, Schoofs H, Castro M, Sabata H, Potente M, Graupera M, Makinen T, Benedito R (2024) iSuRe-HadCre is an essential tool for effective conditional genetics. Nucleic Acids Res 52(13):e56. https://doi.org/10.1093/nar/gkae472
25. KaramanS, Paavonsalo S, Heinolainen K, Lackman MH, Ranta A, Hemanthakumar KA, Kubota Y, Alitalo K (2022) Interplay of vascular endothelial growth factor receptors in organ-specific vessel maintenance. J Exp Med https://doi.org/10.1084/jem.20210565
26. Nagy JA, Dvorak AM, Dvorak HF (2007) VEGF-A and the induction of pathological angiogenesis. Annu Rev Pathol 2:251–275. https://doi.org/10.1146/annurev.pathol.2.010506.134925

27. Lee HW, Xu Y, He L, Choi W, Gonzalez D, Jin SW, Simons M (2021) Role of venous endothelial cells in developmental and pathologic angiogenesis. Circulation 144(16):1308–1322. https://doi.org/10.1161/CIRCULATIONAHA.121.054071
28. Park H, Furtado J, Poulet M, Chung M, Yun S, Lee S, Sessa WC, Franco CA, Schwartz MA, Eichmann A (2021) Defective Flow-Migration coupling causes arteriovenous malformations in hereditary hemorrhagic telangiectasia. Circulation 144(10):805–822. https://doi.org/10.1161/CIRCULATIONAHA.120.053047
29. Xu C, Hasan SS, Schmidt I, Rocha SF, Pitulescu ME, Bussmann J, Meyen D, Raz E, Adams RH, Siekmann AF (2014) Arteries are formed by vein-derived endothelial tip cells. Nat Commun 5:5758. https://doi.org/10.1038/ncomms6758
30. Barbacena P, Dominguez-Cejudo M, Fonseca CG, Gomez-Gonzalez M, Faure LM, Zarkada G, Pena A, Pezzarossa A, Ramalho D, Giarratano Y, Ouarne M, Barata D, Fortunato IC, Misikova LH, Mauldin I, Carvalho Y, Trepat X, Roca-Cusachs P, Eichmann A, Bernabeu MO, Franco CA (2022) Competition for endothelial cell Polarity drives vascular morphogenesis in the mouse retina. Dev Cell 57(19):2321–2333e2329. https://doi.org/10.1016/j.devcel.2022.09.002
31. Boscaro C, Carotti M, Albiero M, Trenti A, Fadini GP, Trevisi L, Sandona D, Cignarella A, Bolego C (2020) Non-genomic mechanisms in the Estrogen regulation of glycolytic protein levels in endothelial cells. FASEB J 34(9):12768–12784. https://doi.org/10.1096/fj.202001130R
32. Cheng N, Trejo J (2023) An SiRNA library screen identifies CYLD and USP34 as deubiquitinases that regulate GPCR-p38 MAPK signaling and distinct inflammatory responses. J Biol Chem 299(12):105370. https://doi.org/10.1016/j.jbc.2023.105370
33. Gao J, Gao Z (2024) The regulatory role and mechanism of USP14 in endothelial cell pyroptosis induced by coronary heart disease. Clin Hemorheol Microcirc 86(4):495–508. https://doi.org/10.3233/CH-232003
34. Huang C, Wang W, Huang H, Jiang J, Ding Y, Li X, Ma J, Hou M, Pu X, Qian G, Lv H (2023) Kawasaki disease: ubiquitin-specific protease 5 promotes endothelial inflammation via TNFalpha-mediated signaling. Pediatr Res 93(7):1883–1890. https://doi.org/10.1038/s41390-022-02341-z
35. Huang H, Huang Y (2024) USP7-stabilised HIPK2 promotes high glucose-induced endothelial cell dysfunctions to accelerate diabetic foot ulcers. Arch Physiol Biochem 130(6):984–991. https://doi.org/10.1080/13813455.2024.2376815
36. Jiang Z, Shen J, Ding J, Yuan Y, Gao L, Yang Z, Zhao X (2021) USP18 mitigates lipopolysaccharide-induced oxidative stress and inflammation in human pulmonary microvascular endothelial cells through the TLR4/NF-kappaB/ROS signaling. Toxicol Vitro 75:105181. https://doi.org/10.1016/j.tiv.2021.105181
37. Lim R, Sugino T, Nolte H, Andrade J, Zimmermann B, Shi C, Doddaballapur A, Ong YT, Wilhelm K, Fasse JWD, Ernst A, Kaulich M, Husnjak K, Boettger T, Guenther S, Braun T, Kruger M, Benedito R, Dikic I, Potente M (2019) Deubiquitinase USP10 regulates Notch signaling in the endothelium. Science 364(6436):188–193. https://doi.org/10.1126/science.aat0778
38. MajumdarU, Manivannan S, Basu M, Ueyama Y, Blaser MC, Cameron E, McDermott MR, Lincoln J, Cole SE, Wood S, Aikawa E, Lilly B, Garg V (2021) Nitric oxide prevents aortic valve calcification by S-nitrosylation of USP9X to activate NOTCH signaling. Sci Adv https://doi.org/10.1126/sciadv.abe3706
39. Shaheen N, Miao J, Li D, Xia B, Baoyinna B, Zhao Y, Zhao J (2024) Indole-3-Acetic acid protects against Lipopolysaccharide-induced endothelial cell dysfunction and lung injury through the activation of USP40. Am J Respir Cell Mol Biol 71(3):307–317. https://doi.org/10.1165/rcmb.2024-0159OC
40. Tang Y, Yuan Q, Zhao C, Xu Y, Zhang Q, Wang L, Sun Z, Cao J, Luo J, Jiao Y (2022) Targeting USP11 May alleviate radiation-induced pulmonary fibrosis by regulating endothelium tight junction. Int J Radiat Biol 98(1):30–40. https://doi.org/10.1080/09553002.2022.1998711
41. Xu C, Wang B, Li M, Dong Z, Chen N, Duan J, Zhou Y, Jin M, Chen R, Yuan W (2024) FUNDC1/USP15/Drp1 ameliorated TNF-alpha-induced pulmonary artery endothelial cell proliferation by regulating mitochondrial dynamics. Cell Signal 113:110939. https://doi.org/10.1016/j.cellsig.2023.110939
42. ZhangW, Qi Y, Wu B (2021) MicroRNA-146-5p promotes pulmonary artery endothelial cell proliferation under hypoxic conditions through regulating USP3. Dis Markers 2021:3668422 https://doi.org/10.1155/2021/3668422
43. Zhao M, Zheng Z, Peng S, Xu Y, Zhang J, Liu J, Pan W, Yin Z, Xu S, Wei C, Wang M, Wan J, Qin JJ (2024) Epidermal growth Factor-Like repeats and discoidin I-Like domains 3 deficiency attenuates dilated cardiomyopathy by inhibiting ubiquitin specific peptidase 10 dependent Smad4 deubiquitination. J Am Heart Assoc 13(6):e031283. https://doi.org/10.1161/JAHA.123.031283
44. Saikia Q, Reeve H, Alzahrani A, Critchley WR, Zeqiraj E, Divan A, Harrison MA, Ponnambalam S (2023) VEGFR endocytosis: implications for angiogenesis. Prog Mol Biol Transl Sci 194:109–139. https://doi.org/10.1016/bs.pmbts.2022.06.021
45. Tammela T, Zarkada G, Wallgard E, Murtomaki A, Suchting S, Wirzenius M, Waltari M, Hellstrom M, Schomber T, Peltonen R, Freitas C, Duarte A, Isoniemi H, Laakkonen P, Christofori G, Yla-Herttuala S, Shibuya M, Pytowski B, Eichmann A, Betsholtz C, Alitalo K (2008) Blocking VEGFR-3 suppresses angiogenic sprouting and vascular network formation. Nature 454(7204):656–660. https://doi.org/10.1038/nature07083
46. Pitulescu ME, Schmidt I, Giaimo BD, Antoine T, Berkenfeld F, Ferrante F, Park H, Ehling M, Biljes D, Rocha SF, Langen UH, Stehling M, Nagasawa T, Ferrara N, Borggrefe T, Adams RH (2017) Dll4 and Notch signalling couples sprouting angiogenesis and artery formation. Nat Cell Biol 19(8):915–927. https://doi.org/10.1038/ncb3555
47. Berlin I, Higginbotham KM, Dise RS, Sierra MI, Nash PD (2010) The deubiquitinating enzyme USP8 promotes trafficking and degradation of the chemokine receptor 4 at the sorting endosome. J Biol Chem 285(48):37895–37908. https://doi.org/10.1074/jbc.M110.129411
48. Ye X, Wang Y, Cahill H, Yu M, Badea TC, Smallwood PM, Peachey NS, Nathans J (2009) Norrin, frizzled-4, and Lrp5 signaling in endothelial cells controls a genetic program for retinal vascularization. Cell 139(2):285–298. https://doi.org/10.1016/j.cell.2009.07.047
49. Zhang C, Lai MB, Khandan L, Lee LA, Chen Z, Junge HJ (2017) Norrin-induced Frizzled4 endocytosis and endo-lysosomal trafficking control retinal angiogenesis and barrier function. Nat Commun 8:16050. https://doi.org/10.1038/ncomms16050
50. Mukai A, Yamamoto-Hino M, Awano W, Watanabe W, Komada M, Goto S (2010) Balanced ubiquitylation and deubiquitylation of frizzled regulate cellular responsiveness to Wg/Wnt. EMBO J 29(13):2114–2125. https://doi.org/10.1038/emboj.2010.100
51. Dudley AC, Griffioen AW (2023) Pathological angiogenesis: mechanisms and therapeutic strategies. Angiogenesis 26(3):313–347. https://doi.org/10.1007/s10456-023-09876-7
52. Liu ZL, Chen HH, Zheng LL, Sun LP, Shi L (2023) Angiogenic signaling pathways and anti-angiogenic therapy for cancer. Signal Transduct Target Ther 8(1):198. https://doi.org/10.1038/s41392-023-01460-1
53. Colombo M, Vallese S, Peretto I, Jacq X, Rain JC, Colland F, Guedat P (2010) Synthesis and biological evaluation of 9-oxo-9H-indeno[1,2-b]pyrazine-2,3-dicarbonitrile analogues as

potential inhibitors of deubiquitinating enzymes. ChemMedChem 5(4):552–558. https://doi.org/10.1002/cmdc.200900409

54. Xie F, Zhou X, Li H, Su P, Liu S, Li R, Zou J, Wei X, Pan C, Zhang Z, Zheng M, Liu Z, Meng X, Ovaa H, Ten Dijke P, Zhou F, Zhang L (2022) USP8 promotes cancer progression and extracellular vesicle-mediated CD8+T cell exhaustion by deubiquitinating the TGF-beta receptor tbetarii. EMBO J 41(16):e108791. https://doi.org/10.15252/embj.2021108791
55. Xiong W, Gao X, Zhang T, Jiang B, Hu MM, Bu X, Gao Y, Zhang LZ, Xiao BL, He C, Sun Y, Li H, Shi J, Xiao X, Xiang B, Xie C, Chen G, Zhang H, Wei W, Freeman GJ, Shu HB, Wang H, Zhang J (2022) USP8 Inhibition reshapes an inflamed tumor microenvironment that potentiates the immunotherapy. Nat Commun 13(1):1700. https://doi.org/10.1038/s41467-022-29401-6
56. Apte RS, Chen DS, Ferrara N (2019) VEGF in signaling and disease: beyond discovery and development. Cell 176(6):1248–1264. https://doi.org/10.1016/j.cell.2019.01.021